# Metal−Organic Framework Co-MOF-74-Based Host−Guest Composites for Resistive Gas Sensing

Ina Strauss,*,[†] Alexander Mundstock,[†] Marvin Treger,[†] Karsten Lange,[†] Seungtaik Hwang,[‡] Christian Chmelik,[‡] Pascal Rusch,[†] Nadja C. Bigall,[†,§] Thomas Pichler,[∥] Hidetsugu Shiozawa,[∥,⊥] and Jürgen Caro*,[†]

[†]Institute of Physical Chemistry and Electrochemistry, Leibniz Universität Hannover, Callinstraße 3A, D-30167 Hanover, Germany
[‡]Faculty of Physics and Earth Sciences, Universität Leipzig, Linnéstraße 5, D-04103 Leipzig, Germany
[§]Laboratory for Nano and Quantum Engineering, Leibniz University Hannover, Schneiderberg 39, D-30167 Hanover, Germany
[∥]Faculty of Physics, University of Vienna, Boltzmanngasse 5, A-1090 Vienna, Austria
[⊥]J. Heyrovsky Institute of Physical Chemistry, Czech Academy of Sciences, Dolejskova 3, CZ-18223 Prague 8, Czech Republic

Ⓢ *Supporting Information*

**ABSTRACT:** Increasing demands in the field of sensing, especially for gas detection applications, require new approaches to chemical sensors. Metal−organic frameworks (MOFs) can play a decisive role owing to their outstanding performances regarding gas selectivity and sensitivity. The tetrathiafulvalene (TTF)-infiltrated MOF, Co-MOF-74, has been prepared following the host−guest concept and evaluated in resistive gas sensing. The Co-MOF-74-TTF crystal morphology has been characterized via X-ray diffraction and scanning electron microscopy, while the successful incorporation of TTF into the MOF has been validated via X-ray photoemission spectroscopy, thermogravimetric analysis, UV/vis, infrared (IR), and Raman investigations. We demonstrate a reduced yet ample uptake of $CO_2$ in the pores of the new material by IR imaging and adsorption isotherms. The nanocomposite Co-MOF-74-TTF exhibits an increased electrical conductivity in comparison to Co-MOF-74 which can be influenced by gas adsorption from a surrounding atmosphere. This effect could be used for gas sensing.



**KEYWORDS:** infiltration of MOFs, Guest@MOF, conducting MOFs, gas sensing, tetrathiafulvalene
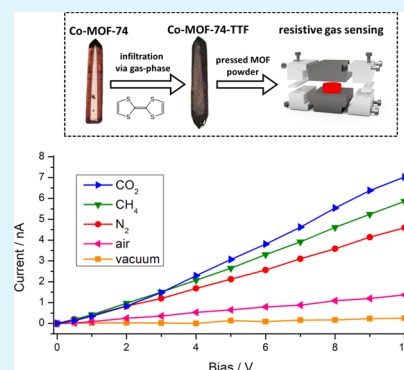
## INTRODUCTION

Metal−organic frameworks (MOFs) are a class of crystalline and porous organic−inorganic hybrid materials.[1,2] A MOF consists of metal ions or metal-oxide clusters as inorganic building units which are connected by organic ligands acting as linkers. The intrinsic porosity of the framework qualifies MOFs for applications like catalysis, drug-delivery systems, gas separation, storage, or sensing.[3−8]

The use of MOFs for the latter has recently gathered increasing attention.[3−9] New chemical sensors are needed for various controlling systems or devices including smart network-connected medical devices or automated industrial process monitoring systems.[10] Today, metal oxides are widely used in chemical sensors leading to problems like atypical operation temperature above 200 °C to promote surface reactions, cross selectivity, and baseline drifts because of aging effects.[11] The use of MOFs for sensing applications could solve those problems by taking advantage of their selective gas adsorption at room temperature.[5,8] There are several concepts for MOF-based gas sensors like colorimetric or resistive sensing applications.[12−15] Here, resistive sensor devices have the advantages that they enable the use of MOF powders in

the form of tablets, making them simple to construct and produce.[9,16] The major bottle neck for the construction of MOF-based resistive gas sensors is the development of electrically conductive or semiconductive MOFs.[17−22] In 2014, Allendorf and co-workers published an electrically conductive MOF based on HKUST-1 doped with the organic semiconductor 7,7,8,8-tetracyanoquinodimethane (TCNQ).[23−25] This was the first conductive MOF following the Guest@MOF concept which is based on the idea that the combination of MOFs and guest molecules can promote new materials with new properties.[25,26] This concept led to the development of conductive composite materials based on MOFs infiltrated with organic semiconductors.[27−29]

Co-MOF-74, also known as CPO-27-Co or $Co_2$(dobdc), contains $Co^{II}$ as metal ions connected through 2,5-dioxido-1,4-benzenedicarboxylate as organic ligands. This MOF-74 possesses a one-dimensional pore system with a pore diameter of 1.1−1.2 nm.[30,31]
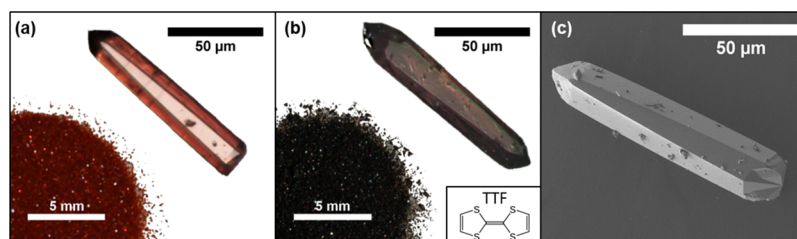
**Figure 1.** Optical microscopy images of powder and single crystals of Co-MOF-74 (a) as well as Co-MOF-74-TTF (b) and the SEM image of Co-MOF-74-TTF (c).
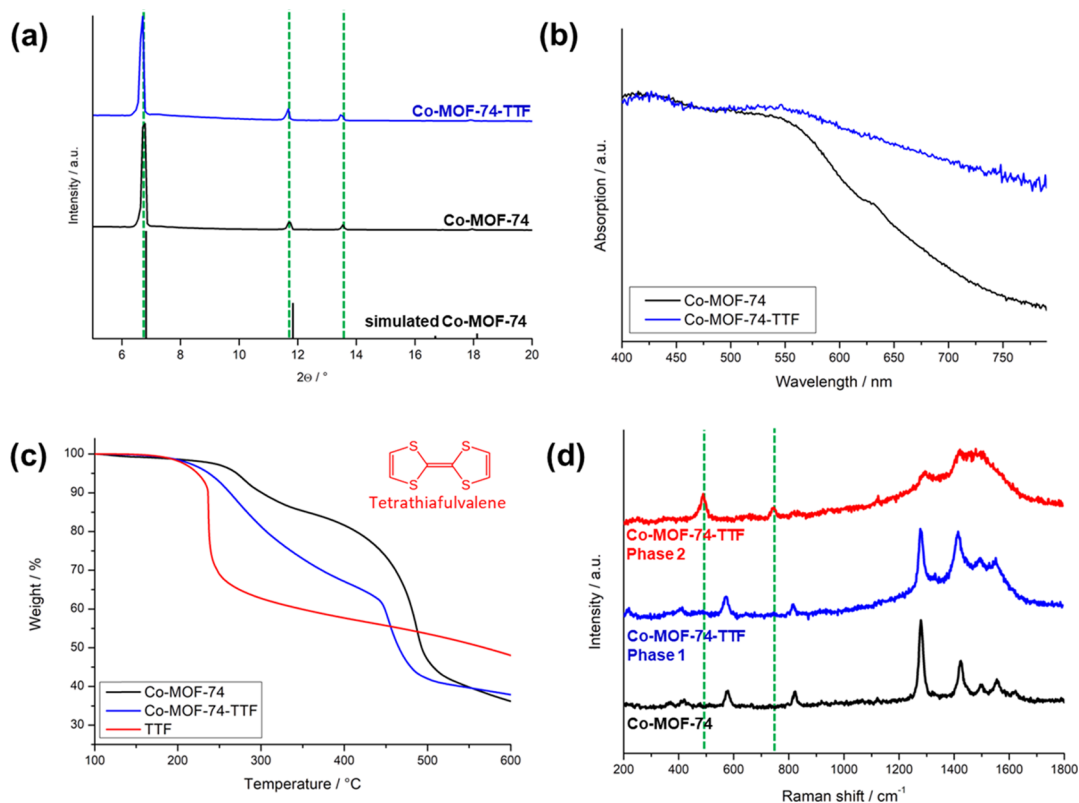


**Figure 2.** (a) XRD data of Co-MOF-74 and Co-MOF-74-TTF compared to the simulated Co-MOF-74 pattern. (b) UV/vis-spectra of Co-MOF-74 compared to Co-MOF-74 infiltrated with TTF. (c) Normalized TGA measurements of Co-MOF-74, Co-MOF-74-TTF, and TTF under the $N_2$ atmosphere. (d) Spatially resolved Raman spectra of Co-MOF-74 showing two different Co-MOF-74-TTF phases at room temperature under vacuum.

In our previous work, we showed that Co-MOF-74, with its hexagonal honeycomb-like lattice and open metal sites, is a potential material for gas sensing.[32]

Here, we present a novel Co-MOF-74-based composite material for gas sensing applications. Following the Guest@ MOF concept, we infiltrated Co-MOF-74 powder with the organic semiconductor tetrathiafulvalene (TTF).[33] Subsequently, resistive gas sensing experiments with pressed tablets were performed.

### ■ EXPERIMENTAL SECTION

**Materials.** All chemicals were received from commercial vendors and used without further purification. For the following synthesis, cobalt nitrate hexahydrate ($Co(NO_3)_2 \cdot 6H_2O$, 99%, Sigma-Aldrich), 2,5-dihydroxy-terephthalic acid (DHBDC, 98%, Sigma-Aldrich), $N,N$-dimethylformamide (DMF, ≥99.8%, Sigma-Aldrich), ethanol (EtOH, ≥99.8%, Sigma-Aldrich), methanol (MeOH, ≥99.8%, Sigma-Aldrich), TCNQ (>98%, TCI), TTF (>98%, TCI), and water ($H_2O$, Millipore) were used.

**Preparation of Co-MOF-74 Powders.** The MOF-74 powders were prepared according to a slightly modified procedure previously published by Chmelik et al.[34] All MOF-74 syntheses were performed in 60 mL Teflon-lined autoclaves (Parr Germany). The metal salt (0.713 g, 2.45 mmol $Co(NO_3)_2 \cdot 6H_2O$) was dissolved in a mixture of DMF, EtOH, and $H_2O$ (60 mL, v/v/v, 1/1/1) and DHBDC (0.145 g, 0.73 mmol) was added. The resulting suspension was ultrasonicated until the solution turns clear and heated for 24 h at 121 °C. After cooling down to room temperature, the precipitate was obtained by centrifugation and washed/solvent-exchanged with MeOH three times. The received solid was dried under reduced pressure and activated under vacuum at 160 °C for 4 h.

**Loading of the MOF.** The MOF powders were infiltrated with the organic semiconductors TCNQ or TTF via the gas phase by storing them in a previously evacuated flask over the respective organic semiconductor molecules at 70 °C overnight, followed by a stepwise increase of the temperature up to 170 °C within 4 h. Afterward, the resulting solid composites were washed with MeOH, dried under reduced pressure, and activated before gas sensing under vacuum at 160 °C over 4 h.

**Characterization of the Materials.** X-ray diffraction (XRD) (Bruker D8 Advance, Cu K$\alpha_1$ radiation $\lambda$ = 0.154 nm) and infrared (IR) spectroscopy (Agilent Technologies Cary 630 FTIR) were used to characterize the MOF powders. The crystal morphologies of the materials were analyzed with optical microscopy (Bruker Senterra Raman spectrometer) and scanning electron microscopy (SEM) (JEOL JSM-6700F NT, 2 kV acceleration voltage). UV/vis measurements were performed using a Cary 5000 UV/vis absorption spectrophotometer from Agilent Technologies. Both samples were measured in an integrating sphere (Agilent DRA-2500) in the reflection mode with a home-made quartz glass cuvette. All spectra were normalized to the maximum absorbance peak.

Thermogravimetric measurements were carried out on Mettler-Toledo TGA/DSC 3+ between 40 and 600 °C with a heating rate of 1 °C/min under $N_2$ flow (50 mL/min).

Spatially resolved Raman spectra were measured with a Horiba Jobin Yvon LabRAM spectrometer equipped with a Coherent Innova 70 ion laser at a wavelength of 514.5 nm ($E_{ex}$ = 2.41 eV).

IR images and IR absorbance spectra under the $CO_2$ atmosphere were achieved with an IR microscope (Bruker Hyperion 3000) connected to a vacuum Fourier transform IR spectrometer (Bruker Vertex 80v) at room temperature. For the IR images, a focal plane array detector was used consisting of an array of 128 × 128 single detectors with a size of 40 × 40 $\mu$m each. By increasing the magnification power of the scanning objective (15 times), a resolution of approximately 2.7 × 2.7 $\mu$m was obtained. The transfer of the crystals into an IR optical cell was carried out inside a glove box under an Ar atmosphere in order to prevent air contact. Subsequently, the cell was connected to the static vacuum system consisting of a pumping station (Pfeiffer Vacuum HiCube 80 Classic) and stainless-steel cylindrical gas reservoirs.

$CO_2$ adsorption isotherms were measured by 3P INSTRUMENTS (Odelzhausen, Germany).

X-ray photoemission spectroscopy (XPS) experiments were performed using a Scienta RS4000 hemispherical analyzer with a monochromatic Al K$\alpha$ X-ray source (1486.6 eV). Toluene solutions containing the MOF crystals were drop-cast onto a gold substrate. Gold 4f lines were used to calibrate the binding energy.

Conductivity measurements were performed in a three-necked glass flask with a home-built electrode setup under atmospheric pressure of the respective gases. Therefore, 0.1 g of each MOF powder was pressed resulting in 0.1 cm thin tablets which were placed between the electrodes. The measurement cell was evacuated for 1 h at 100 °C. Subsequently, I−V curves were recorded by a potentiostat (Bio-Logic VMP3) in the two-electrode configuration. Alternatively, the three-necked glass flask was flushed with nitrogen, methane, or carbon dioxide by a gas flow rate of 30 mL·min$^{-1}$. After every measurement, the glass flask was evacuated for 30 min.

## ■ RESULTS AND DISCUSSION

Figure 1 shows the optical microscopy images of Co-MOF-74 and Co-MOF-74-TTF (Figure 1a,b). The as-synthesized Co-MOF-74 powder shows a red color (Figure 1a), whereas the infiltrated MOF powder appears to be black (Figure 1b). Figure 1c displays an SEM image of a typical Co-MOF-74-TTF crystal. The rodlike crystal has a width of 20 $\mu$m and a length of 70 $\mu$m. The one-dimensional pores of Co-MOF-74 with a diameter of 1.1−1.2 nm are aligned parallel to the long crystal axis.[32]

In order to characterize the crystal structure of Co-MOF-74-TTF, XRD was performed. Figure 2a compares the XRD patterns of Co-MOF-74 and Co-MOF-74-TTF to the simulated Co-MOF-74 pattern. The crystal structure of the infiltrated MOF is almost equal to the noninfiltrated Co-MOF-74. However, a slight shift to a lower 2$\theta$ value for the infiltrated MOF is observed. The UV/vis spectra of the MOFs are shown in Figure 2b. A higher absorption for Co-MOF-74-TTF within

600 and 800 nm compared to Co-MOF-74 can be observed. This proves the successful incorporation of TTF guest molecules into the MOF host structure. Another indication for a successful incorporation of TTF into the pore can be found in the IR spectra, measured at room temperature under air, as given in Figure S1 (Supporting Information). Co-MOF-74 shows $\nu$ OH stretching, which can be attributed either to the presence of carboxyl groups or of adsorbed water molecules in the range of 3000−3500 cm$^{-1}$. Because the infiltrated MOF does not show this stretching mode, we assume the TTF molecules to be infiltrated into the pores, causing reduced water adsorption at the open Co metal sites. These assumptions have been validated by thermogravimetric analysis (TGA) (Figure S2, Supporting Information).

The TGA of the empty Co-MOF-74 equilibrated in air shows a weight loss of 26.4% in the temperature range up to 100 °C, which can be assigned to adsorbed water. The Co-MOF-74-TTF sample contains a lower amount of water compared to the noninfiltrated MOF (5.7 %). Figure 2c shows the TGA of Co-MOF-74, Co-MOF-74-TTF, and TTF under the $N_2$ atmosphere. The results are normalized at 100 °C. The TGA curve of the infiltrated MOF is found between the curves of the empty Co-MOF-74 and the pure TTF. From TGA, we calculated a total amount of TTF infiltrated in Co-MOF-74 to be approximately 15 wt %.

Spatially resolved Raman investigations of Co-MOF-74-TTF crystals (Figure 2d) show the existence of two phases in the $\mu$m scale indicating that the TTF distribution is not homogeneous. One phase is in good accordance with the typical Raman patterns of the unloaded Co-MOF-74, while within the second phase, two additional peaks occur, which can be assigned to TTF.[35] The peak at 494 cm$^{-1}$ is associated with the C−S stretching band and the other peak at 743 cm$^{-1}$ is associated with C−H bending.[35] Further Information concerning the measured areas within the crystals can be found in the Supporting Information (Figure S3).

In order to confirm the existence of Co−S bindings in the second phase, XPS investigations were performed. Figure 3 shows the XPS investigations of Co-MOF-TTF and TTF at the S 2p edge. The S 2p spectra after linear background subtraction have been fit with spin−orbit doublets with shared energy difference and the area intensity ratio between the 2p$_{3/2}$
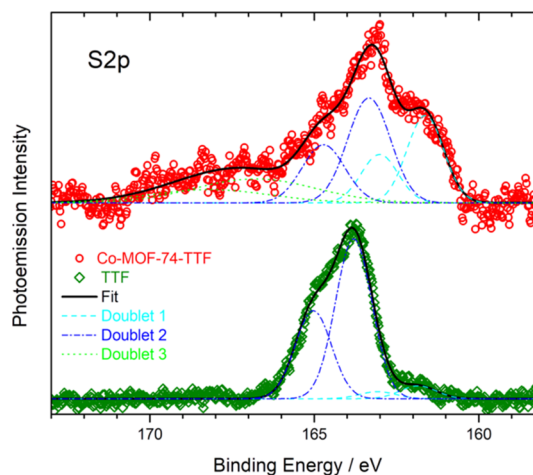


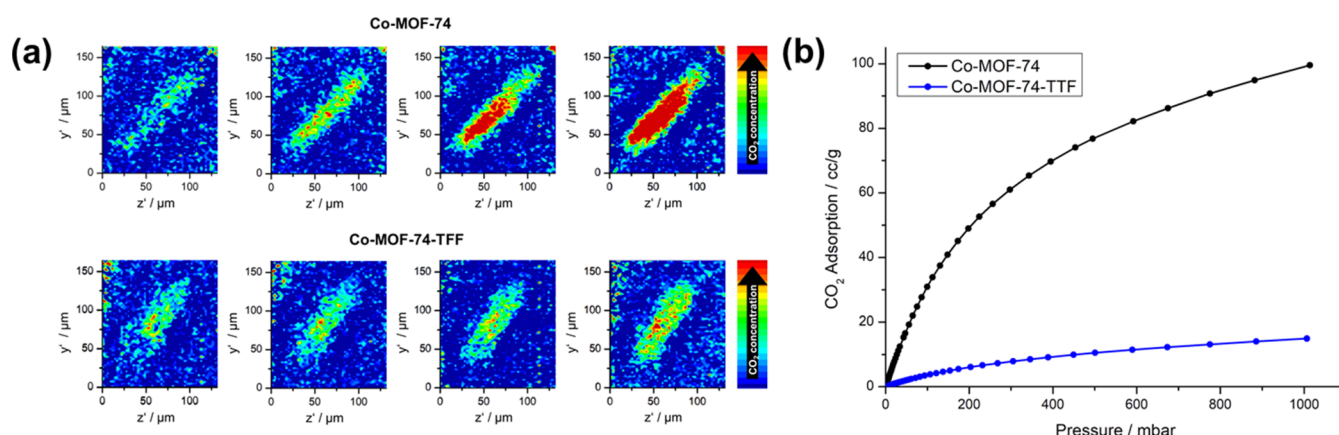**Figure 3.** XPS investigation of Co-MOF-TTF and TTF at the S 2p edge.

**Figure 4.** (a) IR microscopic images of $CO_2$ adsorption on an empty Co-MOF-74 and a composite Co-MOF-74-TTF crystal shown in Figure 1c at 50, 200, 500, and 1000 mbar $CO_2$ pressure (from left to right). (b) $CO_2$ adsorption isotherms of the empty Co-MOF-74 and the composite Co-MOF-74-TTF at 25 °C.

and $p_{1/2}$ Gaussian peaks. For the TTF reference, two doublets can be found. Doublet 1 is low in intensity with the $2p_{3/2}$ peak located at 161.84 eV and doublet 2 is the major component located at 163.80 eV.

For the TTF encapsulated in the Co-MOF-74, doublet 1 is comparable to doublet 2 in intensity. The $2p_{3/2}$ binding energies are downshifted to 161.63 and 163.34 eV for doublets 1 and 2, respectively. In addition, the broad higher energy structure fit as doublet 3 emerges with the $2p_{3/2}$ peak located at 166.80 eV.

The large area intensity of doublet 1 in Co-MOF-74-TTF could be attributed to a sulfur-cobalt bonding state as cobalt sulfide and organic thiols bound on meta surfaces have the S 2p doublet in the same binding energy range.[36−39] The S-to-Co atomic ratio evaluated from the XPS data is approximately 6−7 to 1. Because a TTF molecule contains four sulfur atoms, this means that 1 Co atom interacts with approximately 1.6 TTF molecules (Figure S4, Supporting Information).

IR microscopy images were collected at 50, 200, 500, and 1000 mbar $CO_2$ pressure (Figure 4a). Because the Co-MOF-74 batch consists of equally shaped crystals like the one shown in Figure 1, we can directly compare the IR microscopic images of adsorbed $CO_2$ of the unloaded and the infiltrated Co-MOF-74. For Co-MOF-74, a significant increase of the $CO_2$ uptake is visible when the $CO_2$ pressure inside the cell is increased stepwise from 50 mbar up to 1000 mbar $CO_2$ (from left to right). In contrast to that, Co-MOF-74-TTF does not show a significant increase of $CO_2$ uptake with increasing $CO_2$ pressure because a part of its pore volume is blocked by infiltrating TTF. This finding is in good accordance with the IR absorbance spectra of Co-MOF-74-TTF measured at 10, 20, 50, 100, and 200 mbar $CO_2$ shown in Figure S5 (Supporting Information). The intensity of the $CO_2$ bands does not change when the pressure is varied stepwise from 10 to 200 mbar. It follows from IR imaging (Figure 4a) and IR spectroscopy (Figure S5, Supporting Information) that the $CO_2$ concentration in Co-MOF-74 increases stronger than that in Co-MOF-74-TTF when increasing the $CO_2$ pressure. Therefore, $CO_2$ adsorption isotherms of Co-MOF-74 and Co-MOF-74-TTF, showed in Figure 4b, were measured. On comparing the isotherms, the amount of adsorbed $CO_2$ is drastically reduced in Co-MOF-74-TTF because of the TTF molecules infiltrated into the pores.

As expected, our TTF-infiltrated MOF shows a measurable electric conductivity, similar to that found before for Co-MOF-74 doped with TCNQ.[29] One possible mechanism of the interaction between TTF and Co-MOF-74 might be based on through-bond conduction as suggested for TCNQ-MOFs before.[28] In addition to that, electrons may also conduct through $\pi−\pi$-stacking instead of bond conduction. To check the gas-sensing capability of Co-MOF-74-TTF, the electrical current was measured in dependence of the applied voltage. A measurement setup including a cell for gas sensing was built (Figure 5a). The cell features a gas inlet and outlet for changing the gas atmosphere in the round-bottom flask. The electrode setup (Figure 5b) consists of two stainless-steel electrodes which are held together with screws.

Pressed tablets of the MOF powders are placed between the electrodes, which are connected to the potentiostat with
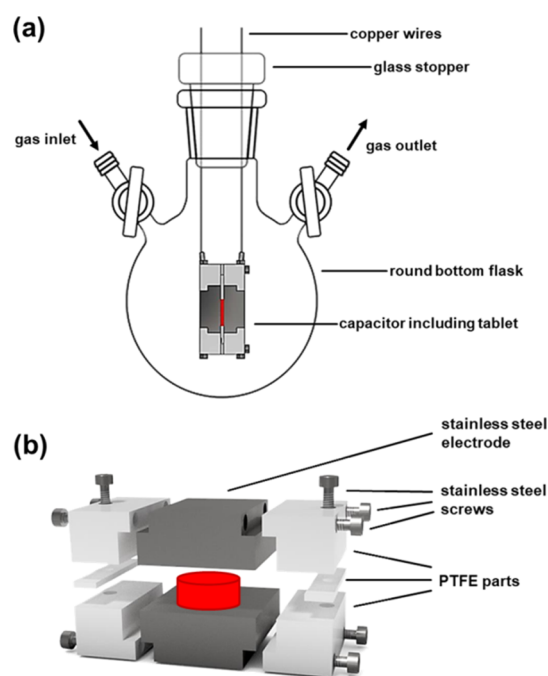


**Figure 5.** Measurement setup (a) and home-build electrodes in detail (b).
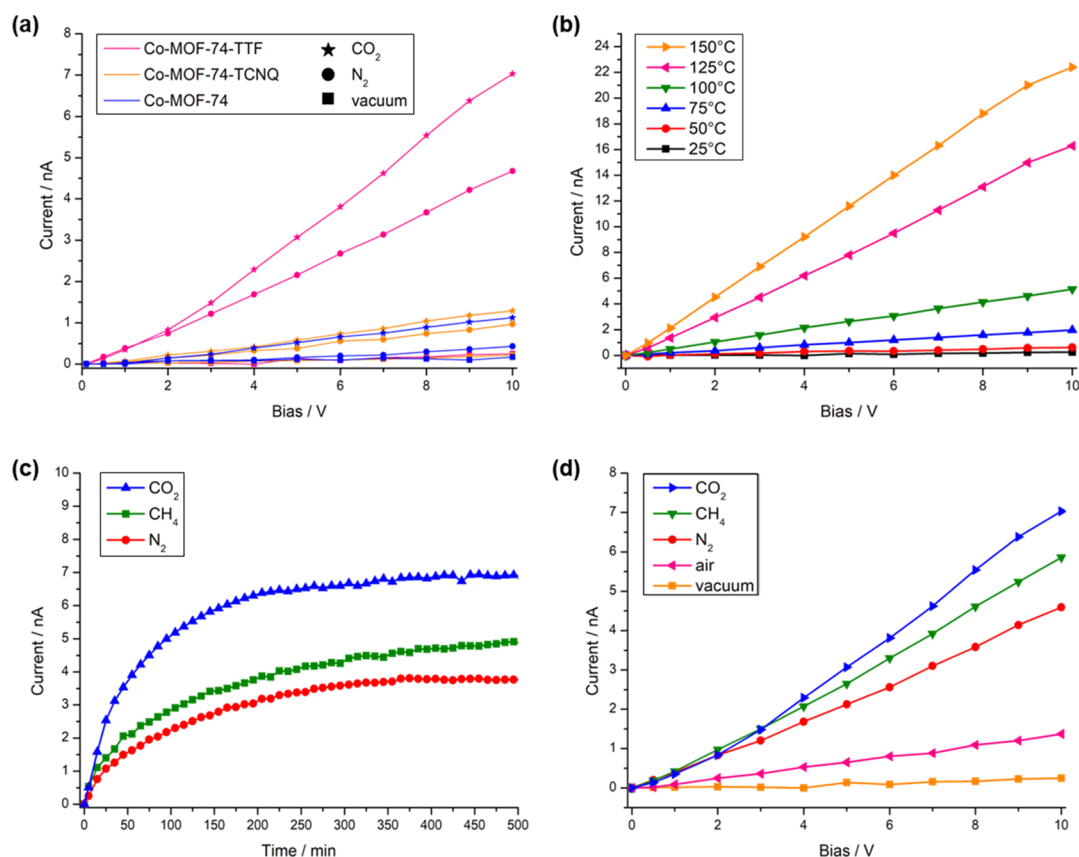
**Figure 6.** Electrical measurements. (a) $I-V$-curves of Co-MOF-74-TTF compared to Co-MOF-74 and Co-MOF-74-TCNQ under vacuum, $N_2$, and $CO_2$ atmospheres. (b) $I-V$-curves of Co-MOF-74-TTF under vacuum at different temperatures. (c) Long-term conductivity measurements of Co-MOF-74-TTF under $N_2$, $CH_4$, and $CO_2$ atmospheres with a bias of 10 V. The atmosphere was changed from vacuum to $N_2/CH_4/CO_2$ at 0 min. (d) $I-V$-curves of Co-MOF-74-TTF measured after 24 h under vacuum, air, $N_2$, $CH_4$, and $CO_2$ atmospheres.

copper wires through the air-tight glass stopper as shown in Figure 5a.

Figure 6a compares the $I-V$ curves of the unloaded Co-MOF-74 with the Co-MOF-74-TTF under vacuum, $N_2$, and $CO_2$. The electrical conductivity of the unloaded Co-MOF-74 is rather low under all conditions. Therefore, Co-MOF-74 is not a suited material for gas sensing via conductivity measurements. Co-MOF-74-TTF, on the other hand, exhibits evaluable electrical conductivity under the $N_2$ and $CO_2$ atmosphere. When compared to the TCNQ-loaded MOF, Co-MOF-74-TTF exhibits a significantly higher electrical conductivity and also larger changes in the conductivity caused by MOF−gas interactions. That is to say, the different gases cause on Co-MOF-74-TTF larger changes in the magnitude of the current and can be distinguished therefrom.

Furthermore, temperature-dependent conductivity measurements of Co-MOF-74-TTF were performed (Figure 6b). Long-time $I-V$ measurements were conducted under $CO_2$, $CH_4$, and $N_2$ at 10 V (Figure 6c). The gas atmosphere was changed from vacuum to different gases at time 0 min. A magnified $I-V$ plot from 0 to 200 s is shown in the Figure S6 (Supporting Information). These short-time measurements show that the TTF-MOF has a short response time regarding the gases.

However, because of transport limitation inside the pressed tablet, no equilibrium of the gas uptake was observed within the first 500 min. Therefore, the following $I-V$ curves were measured 24 h after the initial gas dosing. Figure 6d shows the $I-V$ curves of Co-MOF-74-TTF under vacuum, air, $N_2$, $CH_4$,

and $CO_2$. The highest conductivity was observed for $CO_2$, while the lowest conductivity was found for vacuum. The conductivity under ambient air was low as well.

In a previous publication, we observed shifts of the absorbance maxima in the UV/vis spectra for Co-MOF-74, which were dependent on the strength of the interaction between the MOF and the guest molecules.[32] Here, we observe a similar behavior for the electrical conductivity of the infiltrated MOF. $CO_2$ is interacting stronger with Co-MOF-74-TTF than $CH_4$ and $N_2$.

The interaction of the open metal sites of Co-MOF-74 with $CO_2$ can be further described as a Lewis acid−base interaction, with the metal center acting as a Lewis acid, while the $CO_2$ molecule behaves as an electron donor (Lewis base).[40] This interaction is further favored by the electronic deficiency of the metal sites, leading to a strong interaction between $CO_2$ and the cobalt center.[40] We assume that for Co-MOF-74-TTF, the $CO_2$ molecule, as an electron donor, leads to a higher response compared to $CH_4$ and $N_2$. Garcia et al. stated that the permanent dipole moment, which is present in the cobalt atoms, is able to induce the polarization of molecules like $CH_4$ and showed that the affinity of Co-MOF-74 toward $CH_4$ is lower than toward $CO_2$.[40] For $N_2$, as an inert gas, we assume an even lower interaction. Compared to $CH_4$, $N_2$ also possesses a lower polarizability.[41] These assumptions are in good accordance to the result of the electrical measurements shown in Figure 6d. When Co-MOF-74 is exposed to surrounding air, the conductivity is even lower than for $N_2$. We attribute this low sensitivity to the amount of water in air.

As shown before, Co-MOF-74 can be deactivated by $H_2O$.[33] Thus, it is possible that in Co-MOF-74-TTF, the TTF and $H_2O$ molecules compete for the metal center resulting in lower current. We further investigated the behavior of Co-MOF-74-TTF under vacuum, $CO_2$, and $N_2$ atmospheres via Raman spectroscopy (Figure S7, Supporting Information). When gases become adsorbed in the crystals, gas-specific peak shifts of the characteristic modes of the Co-MOF-74-TTF can be observed. This is in good agreement with the behavior of the noninfiltrated MOF, which showed a shift of the characteristic peaks depending on the applied gas atmosphere as well, justified in more respectively less energetic binding modes.[30]

## CONCLUSIONS

Following the Guest@MOF concept, we synthesized Co-MOF-74 with the organic semiconductor TTF molecules as a host−guest composite via a gas-phase incorporation route. XPS investigations confirm the existence of Co−S bindings (approximately 1.6 TTF molecules interact with 1 cobalt atom) between TTF and the open-metal Co-centers of the MOF. With TGA, we could prove a TTF loading of Co-MOF-74 of 15 wt %.

Co-MOF-74-TTF has a significantly higher conductivity in comparison to the unloaded and TCNQ-infiltrated Co-MOF-74. Furthermore, $I−V$ experiments under different gas atmospheres were performed, recommending Co-MOF-74-TTF as an excellent material for gas-sensing devices because of modification of resistivity. IR imaging and $CO_2$ physisorption show a decreased ability of Co-MOF-74-TTF to adsorb $CO_2$. Because of different strengths of the interactions between a gas and the MOF, conductivity changes could be observed. The highest conductivity was obtained for $CO_2$ because of the strong interaction between $CO_2$ and the Co-centers of the MOF. For weaker gas−MOF interactions ($CO_2 > CH_4 > N_2$), a smaller increase of the conductivity is observed. Raman measurements have proven different interactions of Co-MOF-74-TTF with gas molecules. Peak shifts of the characteristic modes are observed for different gas atmospheres.

## ASSOCIATED CONTENT

### ⓢ Supporting Information

The Supporting Information is available free of charge on the ACS Publications website at DOI: 10.1021/acsami.8b22002.

> Co-MOF-74 IR-spectra compared to Co-MOF-74 infiltrated with TTF; thermogravimetric analysis measurements of Co-MOF-74 and Co-MOF-74-TTF; Co-MOF-74-TTF crystal indicating the two different phases of the material; XPS investigation of Co-MOF-TTF and Co-MOF-74 at the Co 2p edge; IR spectra of Co-MOF-74 and Co-MOF-74-TTF measured at RT with 10, 20, 50, 100, and 200 mbar $CO_2$; and short-time $I−V$ measurements of Co-MOF-74-TTF under $CO_2$, $CH_4$, and $N_2$ (PDF)

## AUTHOR INFORMATION

### Corresponding Authors
*E-mail: ina.strauss@pci.uni-hannover.de (I.S.).
*E-mail: juergen.caro@pci.uni-hannover.de (J.C.).

### ORCID Ⓞ
Ina Strauss: 0000-0001-8824-4162
Karsten Lange: 0000-0002-6741-6911
Nadja C. Bigall: 0000-0003-0171-1106
Thomas Pichler: 0000-0001-5377-9896
Jürgen Caro: 0000-0003-0931-085X

### Notes
The authors declare no competing financial interest.

## REFERENCES

(1) Batten, S. R.; Champness, N. R.; Chen, X.-M.; Garcia-Martinez, J.; Kitagawa, S.; Öhrström, L.; O'Keeffe, M.; Paik Suh, M.; Reedijk, J. Terminology of Metal-Organic Frameworks and Coordination Polymers (IUPAC Recommendations 2013). *Pure Appl. Chem.* **2013**, *85*, 1715−1724.

(2) Yaghi, O. M.; O'Keeffe, M.; Ockwig, N. W.; Chae, H. K.; Eddaoudi, M.; Kim, J. Reticular Synthesis and the Design of new Materials. *Nature* **2003**, *423*, 705−714.

(3) Wang, Z.; Chen, G.; Ding, K. Self-Supported Catalysts. *Chem. Rev.* **2009**, *109*, 322−359.

(4) Wu, M.-X.; Yang, Y.-W. Metal-Organic Framework (MOF)-Based Drug/Cargo Delivery and Cancer Therapy. *Adv. Mater.* **2017**, *29*, 1606134.

(5) Li, J.-R.; Kuppler, R. J.; Zhou, H.-C. Selective Gas Adsorption and Separation in Metal-Organic Frameworks. *Chem. Soc. Rev.* **2009**, *38*, 1477−1504.

(6) Li, Y.-X.; Ji, Y.-N.; Jin, M.-M.; Qi, S.-C.; Li, S.-S.; Xue, D.-M.; Yue, M. B.; Liu, X.-Q.; Sun, L.-B. Controlled Construction of Cu(I) Sites within Confined Spaces via Host-Guest Redox: Highly Efficient Adsorbents for Selective Co Adsorption. *ACS Appl. Mater. Interfaces* **2018**, *10*, 40044−40053.

(7) Morris, R. E.; Wheatley, P. S. Gas Storage in Nanoporous Materials. *Angew. Chem., Int. Ed.* **2008**, *47*, 4966−4981.

(8) Kreno, L. E.; Leong, K.; Farha, O. K.; Allendorf, M.; van Duyne, R. P.; Hupp, J. T. Metal-Organic Framework Materials as Chemical Sensors. *Chem. Rev.* **2012**, *112*, 1105−1125.

(9) Achmann, S.; Hagen, G.; Kita, J.; Malkowsky, I.; Kiener, C.; Moos, R. Metal-Organic Frameworks for Sensing Applications in the Gas Phase. *Sensors* **2009**, *9*, 1574−1589.

(10) Jazdi, N. Cyber physical systems in the context of Industry 4.0. *IEEE International Conference on Automation, Quality and Testing, Robotics (AQTR)*, 2014; pp 1−4.

(11) Capone, S.; Forleo, A.; Francioso, L.; Rella, R.; Siciliano, P.; Spadavecchia, J.; Presicce, D. S.; Taurino, A. M. Solid State Gas Sensors: State of the Art and Future Activities. *Adv. Mater.* **2003**, *5*, 1335−1348.

(12) Razavi, S. A. A.; Masoomi, M. Y.; Morsali, A. Stimuli-Responsive Metal-Organic Framework (MOF) with Chemo-Switchable Properties for Colorimetric Detection of CHCl3. *Chem.—Eur. J.* **2017**, *23*, 12559−12564.

(13) Zhang, Y.; Li, B.; Ma, H.; Zhang, L.; Zhang, W. An RGH-MOF as a naked eye colorimetric fluorescent sensor for picric acid recognition. *J. Mater. Chem. C* **2017**, *5*, 4661−4669.

(14) Smith, M. K.; Jensen, K. E.; Pivak, P. A.; Mirica, K. A. Direct Self-Assembly of Conductive Nanorods of Metal−Organic Frameworks into Chemiresistive Devices on Shrinkable Polymer Films. *Chem. Mater.* **2016**, *28*, 5264−5268.

(15) Campbell, M. G.; Sheberla, D.; Liu, S. F.; Swager, T. M.; Dincă, M. $Cu_3$(hexaiminotriphenylene)$_2$: An Electrically Conductive 2D

Metal-Organic Framework for Chemiresistive Sensing. *Angew. Chem., Int. Ed.* **2015**, *54*, 4349−4352.

(16) Campbell, M.; Dincă, M. Metal-Organic Frameworks as Active Materials in Electronic Sensor Devices. *Sensors* **2017**, *17*, 1108.

(17) Dincă, M.; Léonard, F. Metal−Organic Frameworks for Electronics and Photonics. *MRS Bull.* **2016**, *41*, 854−857.

(18) Leong, C. F.; Usov, P. M.; D'Alessandro, D. M. Intrinsically conducting metal-organic frameworks. *MRS Bull.* **2016**, *41*, 858−864.

(19) Takaishi, S.; Hosoda, M.; Kajiwara, T.; Miyasaka, H.; Yamashita, M.; Nakanishi, Y.; Kitagawa, Y.; Yamaguchi, K.; Kobayashi, A.; Kitagawa, H. Electroconductive Porous Coordination Polymer Cu[Cu(pdt)$_2$] Composed of Donor and Acceptor Building Units. *Inorg. Chem.* **2009**, *48*, 9048−9050.

(20) Gándara, F.; Uribe-Romo, F. J.; Britt, D. K.; Furukawa, H.; Lei, L.; Cheng, R.; Duan, X.; O'Keeffe, M.; Yaghi, O. M. Porous, Conductive Metal-Triazolates and Their Structural Elucidation by the Charge-Flipping Method. *Chem.—Eur. J.* **2012**, *18*, 10595−10601.

(21) Sun, L.; Miyakai, T.; Seki, S.; Dincă, M. Mn2(2,5-disulfhydrylbenzene-1,4-dicarboxylate): A Microporous Metal-Organic Framework with Infinite (−Mn-S−)∞ Chains and High Intrinsic Charge Mobility. *J. Am. Chem. Soc.* **2013**, *135*, 8185−8188.

(22) Darago, L. E.; Aubrey, M. L.; Yu, C. J.; Gonzalez, M. I.; Long, J. R. Electronic Conductivity, Ferrimagnetic Ordering, and Reductive Insertion Mediated by Organic Mixed-Valence in a Ferric Semiquinoid Metal-Organic Framework. *J. Am. Chem. Soc.* **2015**, *137*, 15703−15711.

(23) Talin, A. A.; Centrone, A.; Ford, A. C.; Foster, M. E.; Stavila, V.; Haney, P.; Kinney, R. A.; Szalai, V.; El Gabaly, F.; Yoon, H. P.; Léonard, F.; Allendorf, M. D. Tunable Electrical Conductivity in Metal-Organic Framework Thin-Film Devices. *Science* **2014**, *343*, 66−69.

(24) Chui, S. S. Chemically Functionalizable Nanoporous Material [Cu$_3$(TMA)$_2$(H$_2$O)$_3$]$_n$. *Science* **1999**, *283*, 1148−1150.

(25) Kepler, R. G.; Bierstedt, P. E.; Merrifield, R. E. Electronic Conduction and Exchange Interaction in a New Class of Conductive Organic Solids. *Phys. Rev. Lett.* **1960**, *5*, 503−504.

(26) Allendorf, M. D.; Foster, M. E.; Léonard, F.; Stavila, V.; Feng, P. L.; Doty, F. P.; Leong, K.; Ma, E. Y.; Johnston, S. R.; Talin, A. A. Guest-Induced Emergent Properties in Metal-Organic Frameworks. *J. Phys. Chem. Lett.* **2015**, *6*, 1182−1195.

(27) Sengupta, A.; Datta, S.; Su, C.; Herng, T. S.; Ding, J.; Vittal, J. J.; Loh, K. P. Tunable Electrical Conductivity and Magnetic Property of the Two Dimensional Metal Organic Framework [Cu(TPyP)-Cu$_2$(O$_2$CCH$_3$)$_4$]. *ACS Appl. Mater. Interfaces* **2016**, *8*, 16154−16159.

(28) Guo, Z.; Panda, D. K.; Gordillo, M. A.; Khatun, A.; Wu, H.; Zhou, W.; Saha, S. Lowering Band Gap of an Electroactive Metal-Organic Framework via Complementary Guest Intercalation. *ACS Appl. Mater. Interfaces* **2017**, *9*, 32413−32417.

(29) Shiozawa, H.; Bayer, B. C.; Peterlik, H.; Meyer, J. C.; Lang, W.; Pichler, T. Doping of Metal-Organic Frameworks Towards Resistive Sensing. *Sci. Rep.* **2017**, *7*, 2439.

(30) Rosi, N. L.; Kim, J.; Eddaoudi, M.; Chen, B.; O'Keeffe, M.; Yaghi, O. M. Rod Packings and Metal−Organic Frameworks Constructed from Rod-Shaped Secondary Building Units. *J. Am. Chem. Soc.* **2005**, *127*, 1504−1518.

(31) Dietzel, P. D. C.; Georgiev, P. A.; Eckert, J.; Blom, R.; Strässle, T.; Unruh, T. Interaction of hydrogen with accessible metal sites in the metal-organic frameworks M2(dhtp) (CPO-27-M; M = Ni, Co, Mg). *Chem. Commun.* **2010**, *46*, 4962−4964.

(32) Strauss, I.; Mundstock, A.; Hinrichs, D.; Himstedt, R.; Knebel, A.; Reinhardt, C.; Dorfs, D.; Caro, J. Vis/NIR- und Raman-Untersuchung der Wechselwirkung von Gastmolekülen mit Co-MOF-74. *Angew. Chem. Int. Ed.* **2018**, *130*, 7434−7439.

(33) Wudl, F.; Wobschall, D.; Hufnagel, E. J. Electrical conductivity by the bis(1,3-dithiole)-bis(1,3-dithiolium) system. *J. Am. Chem. Soc.* **1972**, *94*, 670−672.

(34) Chmelik, C.; Mundstock, A.; Dietzel, P. D. C.; Caro, J. Idiosyncrasies of Co$_2$(dhtp): In Situ-Annealing by Methanol. *Microporous Mesoporous Mater.* **2014**, *183*, 117−123.

(35) Adeel, S. M.; Martin, L. L.; Bond, A. M. Redox-induced solid-solid state transformation of tetrathiafulvalene (TTF) microcrystals into mixed-valence and π-dimers in the presence of nitrate anions. *J. Solid State Electrochem.* **2014**, *18*, 3287−3298.

(36) Moulder, J. F.; Stickle, W. F.; Sobol, P. E.; Bomben, K. D. *Handbook of X-ray Photoelectron Spectroscopy*; PerkinElmer Corporation: Eden Prairie, 1992; p 61.

(37) Castner, D. G.; Hinds, K.; Grainger, D. W. X-ray Photoelectron Spectroscopy Sulfur 2p Study of Organic Thiol and Disulfide Binding Interactions with Gold Surfaces. *Langmuir* **1996**, *12*, 5083−5086.

(38) Rufael, T. S.; Huntley, D. R.; Mullins, D. R.; Gland, J. L. Methyl Thiolate on Ni(111): Multiple Adsorption Sites and Mechanistic Implications. *J. Phys. Chem.* **1995**, *99*, 11472−11480.

(39) Mullins, D. R.; Lyman, P. F. Adsorption and reaction of methanethiol on tungsten(001). *J. Phys. Chem.* **1993**, *97*, 9226−9232.

(40) García, E. J.; Mowat, J. P. S.; Wright, P. A.; Pérez-Pellitero, J.; Jallut, C.; Pirngruber, G. D. Role of Structure and Chemistry in Controlling Separations of CO$_2$/CH$_4$ and CO$_2$/CH$_4$/CO Mixtures over Honeycomb MOFs with Coordinatively Unsaturated Metal Sites. *J. Phys. Chem. C* **2012**, *116*, 26636−26648.

(41) Li, J.-R.; Kuppler, R. J.; Zhou, H.-C. Selective Gas Adsorption and Separation in Metal-Organic Frameworks. *Chem. Soc. Rev.* **2009**, *38*, 1477−1504.